Research Article

NEURAL REGENERATION RESEARCH
www.nrronline.org

Erythropoietin inhibits ferroptosis and ameliorates neurological function after spinal cord injury

Yu Kang, Rui Zhu, Shuang Li, Kun-Peng Qin, Hao Tang, Wen-Shan Shan, Zong-Sheng Yin*

https://doi.org/10.4103/1673-5374.353496

Date of submission: January 21, 2022

Date of decision: April 22, 2022

Date of acceptance: June 24, 2022

Date of web publication: September 16, 2022

From the Contents

Graphical Abstract

Erythropoietin inhibits spinal cord injury-induced ferroptosis by enhancing xCT and Gpx4

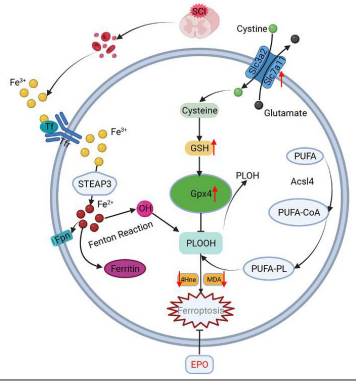

Abstract

Ferroptosis is one of the critical pathological events in spinal cord injury. Erythropoietin has been reported to improve the recovery of spinal cord injury. However, whether ferroptosis is involved in the neuroprotective effects of erythropoietin on spinal cord injury has not been examined. In this study, we established rat models of spinal cord injury by modified Allen's method and intraperitoneally administered 1000 and 5000 IU/kg erythropoietin once a week for 2 successive weeks. Both low and high doses of erythropoietin promoted recovery of hindlimb function, and the high dose of erythropoietin led to better outcome. High dose of erythropoietin exhibited a stronger suppressive effect on ferroptosis relative to the low dose of erythropoietin. The effects of erythropoietin on inhibiting ferroptosis-related protein expression and restoring mitochondrial morphology were similar to those of Fer-1 (a ferroptosis suppressor), and the effects of erythropoietin were largely diminished by RSL3 (ferroptosis activator). *In vitro* experiments showed that erythropoietin inhibited RSL3-induced ferroptosis in PC12 cells and increased the expression of xCT and Gpx4. This suggests that xCT and Gpx4 are involved in the neuroprotective effects of erythropoietin on spinal cord injury. Our findings reveal the underlying anti-ferroptosis role of erythropoietin and provide a potential therapeutic strategy for treating spinal cord injury.

Key Words: erythropoietin; ferroptosis; Gpx4; iron overload; lipid peroxidation; mechanism; neurological function recovery; spinal cord injury; spinal neuron; xCT

Introduction

Spinal cord injury (SCI) is a critical condition that can lead to the irreversible loss of sensorimotor functions, thereby drastically reducing the patient quality of life (Dietz and Fouad, 2014). The initial mechanical damage to spinal cord tissue and the secondary injury, including edema, ischemia, inflammatory response and programmed cell death (PCD), make SCI a refractory disorder (Chen et al., 2020; Shi et al., 2021). Increasing experimental evidence has shown that different types of PCD, such as apoptosis, autophagy, necroptosis, pyroptosis and ferroptosis, play essential roles in SCI (Yong et al., 1998; Wang et al., 2014; Lipinski et al., 2015; Zhang et al., 2019; Xu et al., 2021). Therefore, preventing or alleviating PCD might be a promising strategy for clinical treatment of SCI.

Ferroptosis, a novel type of PCD first proposed by Dixon et al. (2012), is characterized by iron overload, elevated mitochondrial membrane density, accumulated lipid peroxidation and glutathione (GSH) depletion (Dixon et al., 2012; Cao et al., 2020; Jhelum and David, 2022). Transferrin receptor (Tfr) and ferroportin (Fpn) are the proteins involved in iron uptake and exporter respectively (Hentze et al., 2004; Moos et al., 2007). Ferritin heavy chain (Fth) is the subunit of the Ferritin which is the major iron storage protein (Rui et al., 2021). These proteins are responsible for the maintenance of iron homeostasis. Acyl-CoA synthetase long-chain family member 4 (ACSL4) is the key enzyme of lipid peroxidation and 4-hydroxynonenal (4-Hne) is an end-product of lipid peroxidation (Doll et al., 2017; Hassannia et al., 2019). They can reflect the degree of ferroptosis to a certain extent. Glutamate/cystine reverse transporter system Xc^- (xCT) and glutathione peroxidase 4 (Gpx4) are critical to GSH metabolism (Kim et al., 2021). Depletion of xCT and Gpx4 can impair the cellular antioxidant capacity and then lead to ferroptosis (Dixon et al., 2012; Yang et al., 2014). Although ferroptosis was initially defined in cancer cells, recent research has indicated that it is also involved in SCI (Ge et al., 2021, 2022). Bleeding and injury stress contribute to the ferroptosis following SCI. Bleeding caused by contusion is critical in the iron accumulation within the injured spinal cord. Injury stress leads to increased production of reactive oxygen species (ROS) and enhanced excitatory toxicity of glutamate (Chen et al., 2020).

Erythropoietin (EPO) is a cytokine that stimulates the production of erythrocytes. It was primarily used to treat anemia (Wu et al., 1995). With the discovery of EPO receptor in the central nervous system, a neurotherapeutic potential for EPO has emerged (Nagai et al., 2001; Grasso et al., 2005). Several studies confirmed the safety and effectiveness of EPO in treating stroke, epilepsy and Alzheimer's disease (Larpthaveesarp et al., 2016; Sun et al., 2019; Roseti et al., 2020; Ureña-Guerrero et al., 2020). Other studies showed that EPO improved the neurological function of paraplegic animals by regulating PCD following SCI (Yamanaka et al., 2018; Zhong et al., 2020). However, the effects of EPO on ferroptosis in SCI have not been studied.

In this study, we hypothesized EPO could promote neurological function recovery after SCI by alleviating neuronal ferroptosis. In our study, we evaluated the neuroprotective effects of EPO in a SCI rat model, determined the changes of ferroptotic biomarkers, and investigated the regulatory effects of EPO on ferroptosis *in vivo* and *in vitro*.

Department of Orthopedics, The First Affiliated Hospital of Anhui Medical University, Hefei, Anhui Province, China

*Correspondence to: Zong-Sheng Yin, MD, ahmu_zsyin@163.com.

https://orcid.org/0000-0001-9295-3623 (Yu Kang); https://orcid.org/0000-0003-3569-5861 (Rui Zhu); https://orcid.org/0000-0003-4284-1193 (Shuang Li); https://orcid.org/0000-0002-0605-8129 (Kun-Peng Qin); https://orcid.org/0000-0002-8756-3732 (Hao Tang); https://orcid.org/0000-0002-1577-694X (Wen-Shan Shan); https://orcid.org/0000-0002-4862-5443 (Zong-Sheng Yin)

Funding: *This study was supported by the National Natural Science Foundation of China, Nos. 81871785 and 81672161 (both to ZSY).*

How to cite this article: *Kang Y, Zhu R, Li S, Qin KP, Tang H, Shan WS, Yin ZS (2023) Erythropoietin inhibits ferroptosis and ameliorates neurological function after spinal cord injury. Neural Regen Res 18(4):881-888.*

Methods

Animal model

Previous reports indicated that hematuria may be more pronounced in male rats than in female rats, leading to the choice of females in SCI animal models because of fewer urinary tract complications (Ferrero et al., 2015); therefore, we used female rats in our study. Sprague-Dawley rats (*n* = 152, female, specific-pathogen-free, 260–300 g, 6–8 weeks old) were purchased from the Animal Center of Anhui Medical University (license No. SYXK (Wan) 2017-001) and bred in a standard conditions (12-hour light/dark cycle, temperature: 24 ± 2°C, humidity: 60 ± 5%, pathogen-free and free access to food and water). Animals were anesthetized by intraperitoneal injection of 2% sodium pentobarbital (2 mL/kg, Beyotime Biotechnology, Shanghai, China). All experiments and procedures were performed in accordance with the National Institutes of Health Guide for the Care and Use of Laboratory Animals. Animal protocols were approved by the Ethics Committee of Anhui Medical University of China on January 21, 2021 (No. LLSC 20201135).

In the first animal experiment, we used two different doses of EPO (Four Rings Biopharmaceutical Co., Ltd., Beijing, China), referring to previous studies (Freitag et al., 2015; Li et al., 2015; Zhong et al., 2020), to treat the SCI rats. Animals were randomized into four groups (*n* = 5/group): sham (T10 laminectomy with 0.5 mL normal saline), vehicle (SCI with 0.5 mL normal saline), low dose (SCI with 1000 IU/kg EPO), and high dose (SCI with 5000 IU/kg EPO) groups.

In the second experiment, the ferroptosis activator (1S,3R)-RSL3 (RSL3; HY-100218A, MedChemExpress, Shanghai, China) and inhibitor Fer-1 (HY-100579, MedChemExpress) were used. Animals were randomized into five groups (*n* = 5/group): sham (T10 laminectomy with 0.5 mL normal saline), vehicle (SCI with 0.5 mL normaL saline), EPO (SCI with 5000 IU/kg EPO), EPO + RSL3 (SCI with 5000 IU/kg EPO and 5 mg/kg RSL3), and Fer-1 (SCI with 1 mg/kg Fer-1) groups (Yang et al., 2021; Zhou et al., 2021).

To establish the SCI model, modified Allen's method was applied (Zhong et al., 2020). T10 laminectomy was performed to expose the spinal cord and the spinal cord was contused by an impactor (10 g weight × 5 cm height). The sham group was subjected to T10 laminectomy only. The rats were intramuscularly injected with penicillin (infection prevention) and carprofen (pain relief) for the first 3 consecutive days after the operation.

Saline and drugs were intraperitoneally injected immediately postoperatively and once a week for 2 weeks. Animals were sacrificed at designated time points under anesthesia and injured spinal cords were isolated for further tests. The scheme of animal experiments is shown in **Figure 1A**.

Behavioral tests

The Basso, Beattie and Bresnahan (BBB) scale and footprint analysis were performed to assess the hindlimb motor function (Basso et al., 1995; Wen et al., 2015). The BBB scale ranges from 0 (complete hindlimb disability) to 21 points (normal locomotor function). All rats were scored by two researchers who were blinded to animal groups; analyses were performed before surgery and 1, 3, 7 and 14 days post-injury (dpi). For footprint analysis, we made a track (100 cm long and 10 cm wide) with a darkroom at one end to induce rats to walk straight. Footprints were recorded with red ink and white paper (at the bottom of track). The stride length was measured for quantitative analysis.

Magnetic resonance imaging

Magnetic resonance imaging (MRI) was used to evaluate the intraspinal spinal cord at 14 dpi using a 3.0-Tesla MR system (Discovery MR750w, General Electric, Milwaukee, WI, USA) with a rat whole body coil. Sagittal T2 and T2 fat-suppressed images were obtained with the following parameters: repetition time = 4079 ms; echo time = 21 ms; field of view = 10 cm × 8 cm; slice thickness = 1.5 mm.

Histological staining

Pathological changes in the spinal cords of rats were observed by hematoxylin-eosin (HE) staining. Nissl staining was performed to assess neuron survival, and ferric iron was visualized using Perls' Prussian blue staining. Rats were anesthetized and sacrificed at 14 dpi. The spinal cord tissues from the injured epicenter were collected and fixed in 4% paraformaldehyde for 24–48 hours and then dehydrated for 12 hours using an automatic tissue dehydrator (ASP300S, Leica, Solms, Germany). After embedding in paraffin, samples were sliced by a microtome (RM2255, Leica) at 4 μm thickness. Before dewaxing and rehydration, sections were incubated for 2 hours at 60°C. After rehydration, sections were stained by HE Staining Kit (G1120, Solarbio, Beijing, China), Nissl staining solution (G1430, Solarbio) and Perls' Prussian blue Staining Kit (G1422, Solarbio) following the manufacturer's instructions. Finally, sections were dehydrated with gradient alcohol and made transparent with xylene, followed by mounting using neutral gums.

Transmission electron microscopy

Rats at 7 dpi were perfused with 4% paraformaldehyde and spinal cord samples from the injured site were removed. Samples were cut to a size of 1 mm^3 and immersed in fixative solution (paraformaldehyde 2%–glyceraldehyde 2.5% in phosphate-buffered saline (PBS), P885738, Macklin, Shanghai, China) for at least 24 hours. After washing with phosphate buffer solution, the samples were fixed in phosphate buffer with 1% OsO_4 at 4°C for 2 hours and rinsed thoroughly with double-distilled H_2O. The 2% aqueous uranyl acetate was used for *en bloc* staining for 2 hours, and then samples were serially dehydrated with 50%, 70%, 90% and 100% alcohol and 100% acetone and embedded in epoxy resin for making blocks. Silver sections were cut with an ultramicrotome (EM UC7, Leica; thickness 70–90 nm) and stained with lead citrate and uranyl acetate. The sections were observed and imaged with a transmission electron microscope (Talos L120C G2, Thermo Scientific, Waltham, MA, USA).

Tissue iron and reduced GSH assay

Rats at 7 dpi were anesthetized and perfused with pre-cooling sterile saline for removal of erythrocytes in spinal cords. The injured tissue was moved to a sterile glass dish. Spinal dura mater and nerve roots were carefully peeled off. The tissues were homogenized in 9-fold (volume/weight) of normal saline. After centrifugation at 600 × *g* for 10 minutes, the supernatant was collected and assayed with a tissue iron assay kit (A039-2-1) and reduced-GSH assay kit (A006-2-1; Nanjing Jiancheng Bioengineering Institute, Nanjing, China). The optical density (OD) value was measured at 520 nm (for tissue iron) and 405 nm (for GSH). Iron and GSH concentrations were calculated following the manufacturer's instructions.

Malondialdehyde test

Tissue from rats at 7 dpi was collected as described above. Samples were lysed in 9-fold (volume/weight) of cell lysis buffer (P0013, Beyotime Biotechnology) followed by centrifugation at 12,000 × *g* for 10 minutes. All steps were performed at 4°C or on ice. Supernatant was processed using the malondialdehyde (MDA) assay kit (S0131S, Beyotime Biotechnology). The OD value was measured at 532 nm and the MDA concentration was determined by comparing the OD of the standards.

ROS assay

A ROS assay kit (WLA131, WanleiBio, Shenyang, China) was used to detect the ROS content of each group at 7 dpi. After removal of spinal dura mater and nerve roots, spinal cords were homogenized by pipetting in pancreatin for 2 minutes. Homogenate was filtered with a 200 mesh and the cellular suspension was incubated with 2′,7′-dichlorodihydrofluorescein diacetate (DCFH-DA, 10 μM) at 37°C for 25 minutes. Samples were imaged with a microscope (Olympus, Tokyo, Japan) and quantitation of ROS level was analyzed by software ImageJ v1.53c (National Institutes of Health, Bethesda, MD, USA; Schneider et al., 2012).

Quantitative reverse transcription polymerase chain reaction

Spinal cords from rats at 7 dpi were lysed in Trizol (1 mL for 100 mg tissue). Total RNA was extracted with chloroform, precipitated with isopropyl alcohol and rinsed with 75% ethanol. Purity and concentration of RNA were determined following the OD 260/280 nm method (reference value: 1.8–2.0 for purity; 300–400 ng/μL for concentration). Quantitative reverse transcription polymerase chain reaction (qRT-PCR) was performed with the Evo M-MLV RT Master Mix (AG11706, Accurate Biotechnology, Changsha, China) following the manufacturer's instructions; the 10 μL reaction contained 2 μL Evo M-MLV RT Master Mix and 500 ng total RNA in Rnase free water. The reaction conditions were 37°C for 15 minutes, 85°C for 5 seconds and 4°C as the final step. The primers were designed using the BLAST module of NCBI (**Table 1**). qRT-PCR was performed using a 20 μL reaction containing 10 μL 2× SYBR Green Pro Taq HS Premis (AG11701, Accurate Biotechnology), 70 ng complementary DNA, 0.4 μL forward primer, 0.4 μL reverse primer and RNase free water on a LightCycler 96 (Roche, Alameda, CA, USA). The cycling conditions were as follows: 95°C for 5 minutes, followed by 45 cycles of 95°C for 10 seconds, 60°C for 10 seconds and 72°C for 10 seconds, concluding with 95°C for 10 seconds, 65°C for 60 seconds and 97°C for 1 second. All samples were run in duplicate, and the data were quantitated by the $2^{-\Delta\Delta CT}$ method (Livak and Schmittgen, 2001).

Table 1 | **Primer sequence used in quantitative reverse transcription polymerase chain reaction**

Gene	Primer sequence (5'–3')	Product size (bp)
xCT	Forward: GTT CAG ACG ATT GTC AGA CAG AA	189
	Reverse: ACC AAT TCC TTT AGC CCA TCA	
Gpx4	Forward: AGT CCT AGG AAG CGC CCA G	170
	Reverse: CAT CGC GGG ATG CAC ACA AG	
β-Actin	Forward: CAC CAT GTA CCC AGG CAT TG	173
	Reverse: CCT GCT TGC TGA TCC ACA TC	

Gpx4: Glutathione peroxidase 4; xCT: glutamate/cystine reverse transporter system Xc^-.

Cell culture and viability assay

PC12 cells, an alternative cell line for primary neurons (Greene and Tischler, 1976), were purchased from the Cell Resource Center of Shanghai Institute for Biological Science (Shanghai, China, Cat# TCR8, Identifier code: CSTR:19375.09.3101RATTCR8). PC12 cells are widely used as a model cell of neurons to investigate neuronal damage resulting from SCI (Lin et al., 2016; He et al., 2017; Shen et al., 2017). Cells were cultured at 37°C and 5% CO_2 in Roswell Park Memorial Institute 1640 Medium containing 10% fetal bovine serum and 1% penicillin-streptomycin (Gibco, San Diego, CA, USA).

The half maximal inhibitory concentration (IC50) of RSL3 to PC12 cells was evaluated using Cell Counting Kit 8 (C0037, Beyotime Biotechnology). Briefly,

RSL3 was dissolved to 0.5, 1, 2, 5, 10, 20, and 50 mM in dimethylsulfoxide and then diluted by culture medium to 0.5, 1, 2, 5, 10, 20, and 50 μM. Cells seeded in 96-well plates (1×10^4 cells per well) were treated with the gradient concentrations of RSL3. After 24 hours, the culture medium was replaced with 100 μL fresh medium containing 10 μL Cell Counting Kit 8 solution, and cells were incubated at 37°C for 0.5 hour. OD values were measured at 450 nm.

In other experiments, PC12 cells were divided into control, RSL3 and RSL3 + EPO groups. RSL3 was dissolved in dimethylsulfoxide and then diluted by culture medium according to the result of IC_{50}. EPO was directly diluted in culture medium. The final concentration of dimethylsulfoxide was 0.1%. The intervention time was 24 hours, and the control group was treated with 0.1% dimethylsulfoxide.

Mitochondrial membrane potential test

Mitochondrial membrane potential (MMP) of PC12 cells was detected using an enhanced MMP assay kit with JC-1 (C2003S, Beyotime Biotechnology). Cells were incubated with JC-1 working solution (JC-1 200×:JC-1 buffer = 1:200) at 37°C for 25 minutes. An inverted fluorescence microscope (Axio Observer 3, Oberkochen, Germany) was used for observation, and flow cytometry (FCM, Bd Celesta, San Jose, CA, USA) was used for quantitative analysis.

Western blot assay

At 14 dpi, injured spinal cords were collected and weighed. Tissue (20 mg) was lysed in 200 μL radio-immunoprecipitation assay lysis buffer (P0013B, Beyotime Biotechnology) with 1 mM phenylmethanesulfonyl fluoride on ice for 30 minutes. The homogenate was centrifuged at 12,000 × *g* for 15 minutes at 4°C. For cultured cells, cells in each well (6-well plate) were lysed in 200 μL RIPA with 1 mM phenylmethanesulfonyl fluoride. The lysates were centrifuged at 12,000 × *g* for 15 minutes at 4°C. Protein concentration was determined using the BCA assay. Samples were mixed with 5× loading buffer (P0015L, Beyotime Biotechnology, 4:1), denatured at 100°C for 10 minutes, separated by 10% sodium dodecyl sulfate-polyacrylamide gel electrophoresis, and transferred to polyvinylidene fluoride membranes. Membranes were blocked in 5% non-fat milk for 90 minutes at room temperature, followed by incubation overnight at 4°C with primary antibodies against Gpx4 (mouse, 1:2000, Proteintech, Wuhan, China, Cat# 67763-1-Ig, RRID: AB_2909469), xCT (rabbit, 1:2000, Proteintech, Cat# 26864-1-AP, RRID: AB_2880661), 4-Hne (rabbit, 1:3000, Abcam, Cambridge, MA, USA, Cat# ab46545, RRID: AB_722490), Acsl4 (rabbit, 1:1000, Affinity, Changzhou, China, Cat# DF12141, RRID: AB_2844946), Tfr (rabbit, 1:1000, Affinity, Cat# AF5343, RRID: AB_2837828), Fpn (rabbit, 1:1000, Affinity, Cat# DF13561, RRID: AB_2846580), Fth (rabbit, 1:1000, Affinity, Cat# DF6278, RRID: AB_2838244) and glyceraldehyde-3-phosphate dehydrogenase (Gapdh; rabbit, 1:5000, Affinity, Cat# AF7021, RRID: AB_2839421). The membrane was incubated with horseradish peroxidase-conjugated anti-rabbit (1:10,000, Affinity, Cat# S0001, RRID: AB_2839429) or anti-mouse secondary antibodies (1:10,000, Affinity, Cat# S0002, RRID: AB_2839430) at 25°C for 1.5 hours. Protein bands were visualized using an enhanced chemiluminescence system (Epizyme Biotech, Shanghai, China). Quantitation of western blot was performed by software ImageJ v1.53c. Gapdh was used as internal reference.

Immunofluorescence staining

Spinal cord tissues from the injured epicenter were collected at 14 dpi and cut into sections (thickness 4 μm). After dewaxing and rehydration, citrate buffer was used for antigen repair via the microwave thermal repair method. PC12 cells were seeded in 24-well culture plates plated with cell-climbing slices. Slices were fixed with 4% paraformaldehyde for 15 minutes. Tissue sections and slices were blocked and permeabilized in immune staining blocking buffer (P0102, Beyotime Biotechnology) for 50 minutes at 37°C. Sections were incubated overnight at 4°C with primary antibodies against Gpx4 (mouse, 1:200, Proteintech, Cat# 67763-1-Ig, RRID: AB_2909469), xCT (rabbit, 1:200, Proteintech, Cat# 26864-1-AP, RRID: AB_2880661), 4-Hne (rabbit, 1:200, Abcam, Cat# ab46545, RRID: AB_722490), neuronal nuclei (NeuN; rabbit, 1:200, Affinity, Cat# DF6145, RRID: AB_2838112) and Neun (mouse, 1:200, Proteintech, Cat# 66836-1-Ig, RRID: AB_2882179). Samples were then incubated with fluorescence secondary antibody (37°C for 1 hour): fluorescein isothiocyanate (FITC; rabbit, 1:100, ZSGB-BIO, Beijing, China, Cat# ZF-0311, RRID: AB_2571576), FITC (mouse, 1:100, ZSGB-BIO, Cat# ZF-0312, RRID: AB_2716306), tetramethylrhodamine isothiocyanate (TRITC; rabbit, 1:100, ZSGB-BIO, Cat# ZF-0316, RRID: AB_2728778) and TRITC (mouse, 1:100, ZSGB-BIO, Cat# ZF-0313, RRID: AB_2571577). Nuclei were stained in 2-(4-amidinophenyl)-6-indolecarbamidine dihydrochloride (DAPI) staining solution (C1005, Beyotime Biotechnology) at 25°C for 5 minutes. Antifade mounting medium (P0126, Beyotime Biotechnology) was used to seal the sections. The automatic positive fluorescence microscope (DM6B, Leica) was used for pictures and ImageJ software was used for quantitative analysis.

Statistical analysis

No statistical methods were used to predetermine sample sizes; however, our sample sizes are similar to those reported in a previous publication (Gong et al., 2022). No animals or data points were excluded from the analysis. The evaluators were blind to the assignments. Statistical analysis and visualization were performed using GraphPad Prism 8.0.2 software (GraphPad Software, San Diego, CA, USA, www.graphpad.com). Data were analyzed using two-way analysis of variance followed by Tukey's multiple comparisons test or one-way analysis of variance followed by Dunnett's multiple comparisons test. $P < 0.05$ indicated statistical significance.

Results

EPO exhibits a neuroprotective effect in SCI rats

To investigate whether EPO can exhibit a neuroprotective effect in SCI rats, we evaluated the recovery of hindlimb motor function in the four experimental groups using the BBB scale (scored at 1, 3, 7, 14 dpi) and footprint analysis (at 14 dpi). At 1 and 3 dpi, there was no significant difference in BBB score in the two EPO groups relative to that in the vehicle group (low dose *vs*. vehicle: $P = 0.608$; high dose *vs*. vehicle: $P = 0.534$; **Figure 1B**). However, from day 7, the BBB scores in the EPO groups were significantly higher than those of the vehicle group (low dose *vs*. vehicle: $P = 0.022$; high dose *vs*. vehicle: $P < 0.001$). Footprint analysis showed that the stride distance of the EPO groups was remarkably improved, and that the bilateral strides of the EPO groups were more symmetrical than those of the vehicle group (low dose *vs*. vehicle: $P = 0.005$ for left and $P < 0.001$ for right; high dose *vs*. vehicle: $P < 0.001$ for both sides; **Figure 1C** and **D**). The higher BBB score and longer stride distance in the high dose group relative to those in the low dose group indicated that high dose EPO had a better neuroprotective effect on SCI than the low dose ($P < 0.001$).

EPO promotes regeneration of SCI

Histology and neuroimaging were used to evaluate the regeneration of injured spinal cord at 14 dpi. HE staining was performed to observe the tissue damage and repair, and Nissl staining was used to evaluate the loss of spinal neurons. In the high dose group, both tissue morphology and Nissl positive cell number were similar to those in the sham group (**Figure 1E**). MRI scans were performed to evaluate the lesion areas within the spinal cord. Fat-suppressed T2-weighted sagittal MRI showed that the hyperintense area of the lesion in both low and high dose groups were smaller than that in the vehicle group (**Figure 1F**).

EPO alleviates the iron overload within the injured spinal cord

After contusion, subdural bleeding results in accumulation of erythrocytes and hemoglobin around the injured region of the spinal cord, which causes abnormal iron deposition. Perls' Prussian blue staining showed that the number of blue-stained cells markedly increased in the vehicle group after SCI relative to that in the control group; however, there were fewer blue-stained cells in the low and high dose EPO groups (**Figure 2A**). Moreover, while the vehicle group had a much higher level of tissue iron concentration relative to the sham group, the iron concentration decreased with the treatment of EPO ($P < 0.001$; **Figure 2B**).

EPO diminishes the accumulation of ROS and lipid peroxidation in the injured spinal cord

In ferroptosis, iron overload generates highly reactive hydroxyl radicals through the Fenton reaction, which results in the accumulation of ROS and lipid peroxidation (Jing et al., 2021). MDA is a natural product of lipid oxidation in living organisms, reflecting the level of lipid peroxidation. We next evaluated ROS and MDA contents respectively. Fluorescence analysis revealed that the ROS fluorescence intensity in the vehicle group had increased after injury relative to those in the sham group ($P < 0.001$); and the ROS fluorescence intensity was significantly decreased in both the low dose and high dose groups relative to that in the vehicle group (low dose *vs.* vehicle: $P < 0.001$; high dose *vs*. vehicle: $P < 0.001$; **Figure 2C** and **D**). Similarly, MDA content was increased after SCI and diminished by EPO treatment (vehicle *vs.* sham: $P < 0.001$; low dose *vs.* vehicle: $P < 0.001$; high dose *vs.* vehicle: $P < 0.001$; **Figure 2E**).

EPO attenuates SCI-induced expression of ferroptosis markers

Accumulating evidence demonstrates that ferroptosis is involved in neuronal death following SCI (Zhang et al., 2020; Cheng et al., 2021; Feng et al., 2021; Ge et al., 2021). We next examined the expression of the ferroptosis-related proteins Tfr, Fpn, Fth, Acsl4 and 4-Hne in injured spinal cords at 14 dpi (Feng et al., 2020; Cui et al., 2021; Rui et al., 2021) using western blot assay. All markers were increased in the vehicle group relative to those in the sham group (**Figure 3A–H**). We found that 4-Hne was significantly downregulated in both low and high dose EPO groups relative to that in the vehicle group (low dose *vs.* vehicle: $P = 0.001$; high dose *vs*. vehicle: $P < 0.001$), while Tfr, Acsl4, Fpn and Fth were decreased only in the high dose group (Tfr: $P = 0.016$; Acsl4: $P = 0.005$; Fpn: $P = 0.019$; Fth: $P = 0.003$).

EPO upregulates the expression of xCT and Gpx4 and rescues depletion of GSH in SCI

Gpx4, GSH and xCT have a synergistic relationship in the antioxidant system, and their reduction can trigger ferroptosis (Kremer et al., 2021; Lu et al., 2021). The vehicle group showed reduction of GSH and decreased mRNA levels of xCT and Gpx4 at 7 dpi (xCT: $P < 0.001$; Gpx4: $P < 0.001$; **Figure 3I–K**), and western blot analysis showed reduced Gpx4 and xCT at 14 dpi (xCT: $P = 0.001$; Gpx4: $P = 0.001$) (**Figure 3A**, **G–H**). Notably, these changes were partially reversed in the EPO groups. Both doses of EPO significantly enhanced the expressions of xCT and Gpx4 relative to that in the vehicle group (low dose *vs*. vehicle: $P < 0.001$ and $P = 0.044$ for mRNA and protein of xCT, $P = 0.026$ and $P = 0.027$ for mRNA and protein of Gpx4; high dose *vs*. vehicle: $P < 0.001$ for both mRNA and protein of xCT, $P < 0.001$ and $P = 0.003$ for mRNA and protein of Gpx4, **Figure 3A** and **G–J**) and promoted GSH content (low dose *vs.* vehicle: $P = 0.034$; high dose *vs.* vehicle: $P < 0.001$; **Figure 3K**).

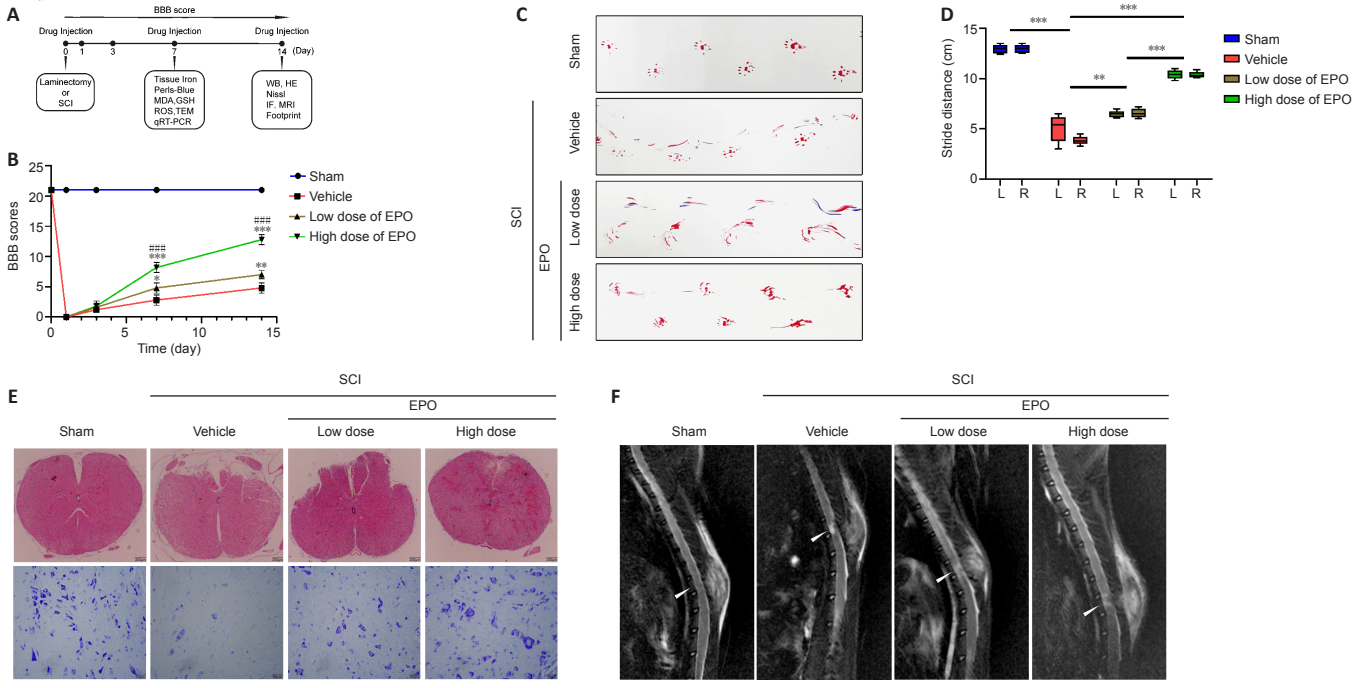

Figure 1 | **EPO promotes hindlimb function recovery and tissue repair after SCI.**
(A) A schematic of the animal experiments. (B) BBB scores of the indicated groups. (C) Footprints of the hindlimb at 14 dpi. (D) The boxplot of stride distance for footprint analysis. (E) HE (top row) and Nissl staining (bottom row) of injured tissue at 14 dpi. Scale bars: top, 200 μm; bottom, 50 μm. (F) MRI of each group at 14 dpi. The arrows indicate the epicenter of lesions. All data are expressed as the mean ± SD (n = 5 in each group). $^{**}P < 0.01$, $^{***}P < 0.001$, *vs.* vehicle group; $^{\#\#\#}P < 0.001$, *vs.* low dose group (two-way analysis of variance followed by Tukey's multiple comparisons test). BBB: Basso, Beattie and Bresnahan locomotor rating scale; dpi: day(s) post injury; GSH: glutathione; HE: hematoxylin eosin; IF: immunofluorescence; MDA: malondialdehyde; L: left; MRI: magnetic resonance imaging; qRT-PCR: quantitative reverse transcription polymerase chain reaction; R: right; ROS: reactive oxygen species; SCI: spinal cord injury; TEM: transmission electron microscope; WB: western blot.

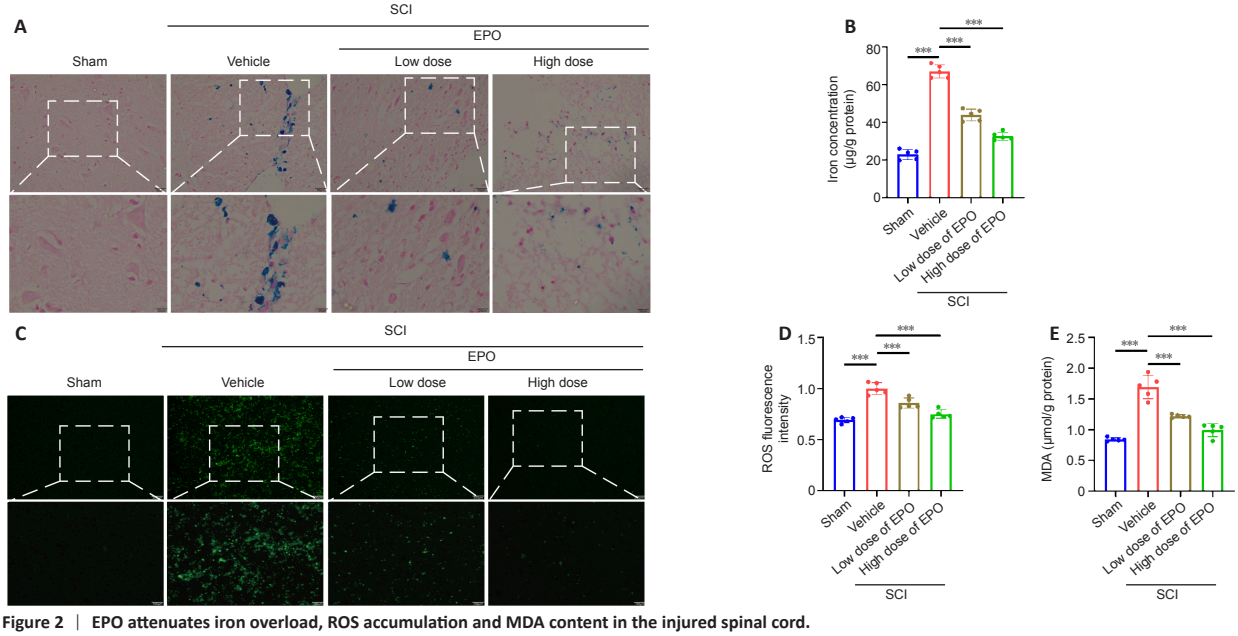

Figure 2 | **EPO attenuates iron overload, ROS accumulation and MDA content in the injured spinal cord.**
(A) Perls' Prussian blue staining of injured tissue at 7 dpi. Iron-positive cells were stained by blue. Scale bars: top, 50 μm; bottom, 25 μm. (B) Iron contents of injured tissue at 7 dpi. (C, D) Fluorescence (C) and quantitation (D) of ROS from injured tissue at 7 dpi. Scale bars: top, 200 μm; bottom, 100 μm. (E) MDA concentration of injured tissue at 7 dpi. All data are expressed as the mean ± SD (n = 5 in each group). $^{***}P < 0.001$ (one-way analysis of variance followed by Dunnett's multiple comparisons test). dpi: Day(s) post injury; MDA: malondialdehyde; ROS: reactive oxygen species; SCI: spinal cord injury.

Neuroprotection of EPO in SCI is largely abolished by the ferroptosis activator RSL3

RSL3 is a ferroptosis activator targeting Gpx4 (Shin et al., 2018), and Fer-1 is a ferroptosis inhibitor (Liu et al., 2020b). We evaluated neuronal function recovery and ferroptosis level in SCI rats treated with EPO, EPO + RLS3 and Fer-1. We further determined the expression of xCT and Gpx4 in spinal neurons using immunofluorescence test. A previous study demonstrated that the Fer-1 ferroptosis inhibitor improved the hindlimb motor function of rats after SCI (Ge et al., 2021). We found that rats treated with EPO achieved similar BBB scores as those treated with Fer-1; both scores were significantly higher than the vehicle group ($P < 0.001$; **Figure 4A**). The BBB score of the EPO + RSL3 group was significantly decreased relative to that of the EPO group ($P < 0.001$) and not significantly different from the vehicle group at 14 dpi ($P = 0.151$).

We next analyzed the expressions of ferroptosis-related proteins. The expressions of Tfr, Fpn and 4-Hne in the EPO and Fer-1 groups were significantly lower than those in the vehicle group, while the expression in the EPO + RSL3 group was increased relative to that in the EPO and Fer-1 groups (EPO *vs.* vehicle: $P < 0.001$ for Tfr and Fpn, $P = 0.005$ for 4-Hne; EPO *vs.* EPO + RSL3: $P = 0.005$ for Tfr, $P = 0.002$ for Fpn, $P = 0.01$ for 4-Hne; Fer-1 *vs.* vehicle: $P < 0.001$ for Tfr and Fpn, $P = 0.005$ for 4-Hne; Fer-1 *vs.* EPO + RSL3: $P = 0.004$ for Tfr, $P = 0.014$ for Fpn, $P = 0.011$ for 4-Hne; **Figure 4B–E**). The expressions of xCT and Gpx4 in the EPO and Fer-1 groups were significantly higher than those in the vehicle and EPO + RSL3 groups, while the expressions in the EPO + RSL3 group were lower relative to those in the EPO and Fer-1 groups (EPO *vs.* vehicle: $P < 0.001$ for xCT and Gpx4; EPO *vs.* EPO + RSL3: $P = 0.001$ for xCT and Gpx4; Fer-1 *vs.* vehicle: $P = 0.001$ for xCT and Gpx4; Fer-1 *vs.* EPO + RSL3: $P = 0.006$ for xCT, $P = 0.002$ for Gpx4; **Figure 4B**, **F–G**).

To further confirm the putative role of EPO on SCI-induced ferroptosis, we used TEM to observe the mitochondrial morphology. Ferroptosis-like morphological changes, characterized by the reduction or vanishing of mitochondria crista and outer mitochondrial membrane rupture (Liu et al., 2020a), were observed in the vehicle group and the EPO + RSL3 group (**Figure 4H**). The mitochondria in the EPO and Fer-1 groups were morphologically closer to those of the sham group.

Our results indicated that EPO attenuated ferroptosis within the local tissue after SCI, but whether EPO exerted its effects via inhibiting neuronal ferroptosis was unclear. Therefore, double-label immunofluorescence of spinal cord sections was used to determine the expression of xCT, Gpx4 and 4-Hne in spinal neurons. There were more cells positive for NeuN (a neuronal marker) in the EPO and Fer-1 groups than the vehicle and EPO + RSL3 groups (**Figure 5**). Furthermore, the fluorescence intensities of xCT and Gpx4 were higher in the EPO and Fer-1 groups relative to that in the vehicle group (xCT: $P < 0.001$ for both EPO and Fer-1; Gpx4: $P = 0.004$ for EPO, $P = 0.011$ for Fer-1), while 4-Hne showed the opposite trend. There were no significant differences in the staining for xCT, Gpx4 and 4-Hne in the EPO + RSL3 and vehicle groups (xCT: $P = 0.998$; Gpx4: $P = 0.273$; 4-Hne: $P = 0.974$). Collectively, our results showed that the therapeutic effect of EPO on SCI rats was related to ferroptosis inhibition which was mediated by upregulating xCT and Gpx4.

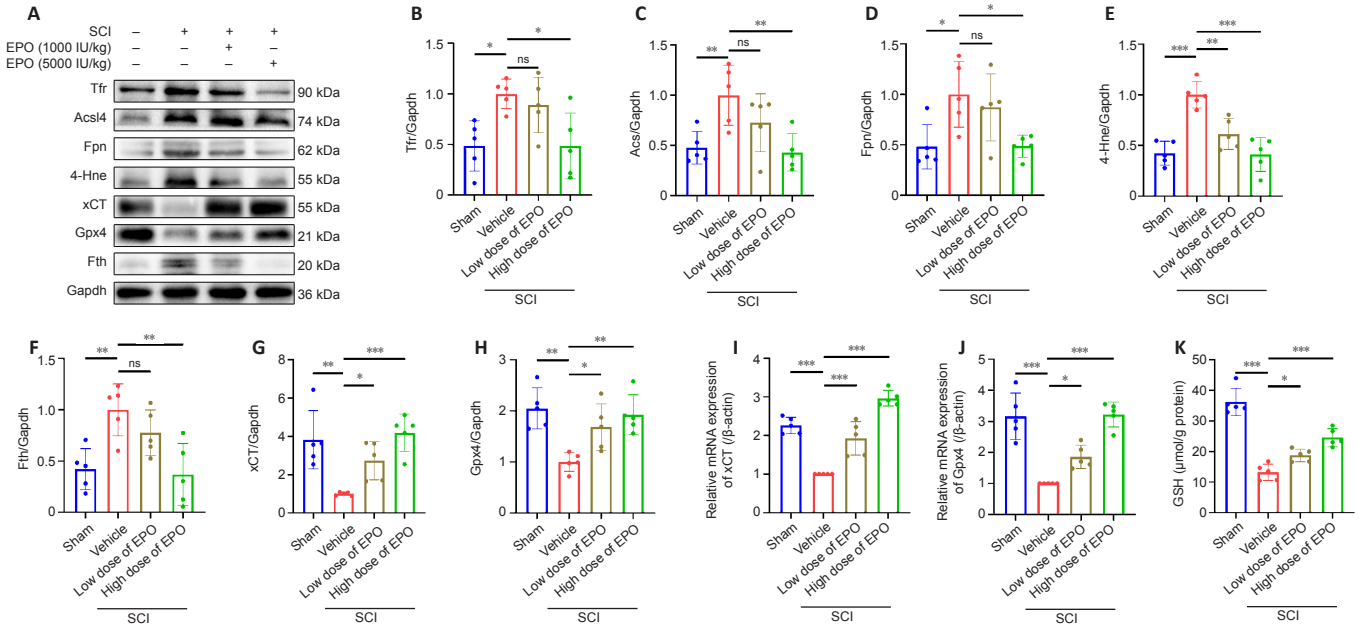

Figure 3 | **EPO regulates the expression of ferroptotic biomarkers after SCI.**
(A) Western blot of the indicated proteins in injured tissues from the treatment groups. (B–H) Quantitative analysis of Tfr, Fpn, Fth, Acsl4 and 4-Hne protein expression at 14 dpi. Gapdh was used as the reference protein. (I, J) Quantitative reverse transcription polymerase chain reaction results of xCT and Gpx4 mRNA extracted from injured tissue at 7 dpi. β-Actin mRNA was used as the reference gene. (K) Quantitative analysis of reduced GSH from injured tissue at 7 dpi. All data are expressed as the mean ± SD ($n = 5$ in each group). $^*P < 0.05$, $^{**}P < 0.01$, $^{***}P < 0.001$ (one-way analysis of variance followed by Dunnett's multiple comparisons test). 4-Hne: 4-Hydroxynonenal; Acsl4: acyl-coenzyme A synthetase long chain family member 4; dpi: day(s) post injury; EPO: erythropoietin; Fpn: ferroportin or solute carrier family 40 member 1; Fth: ferritin heavy chain; Gapdh: glyceraldehyde-3-phosphate dehydrogenase; Gpx4: glutathione peroxidase 4; GSH: glutathione; ns: not significant; SCI: spinal cord injury; Tfr: transferrin receptor; xCT: the solute carrier family 7 member 11.

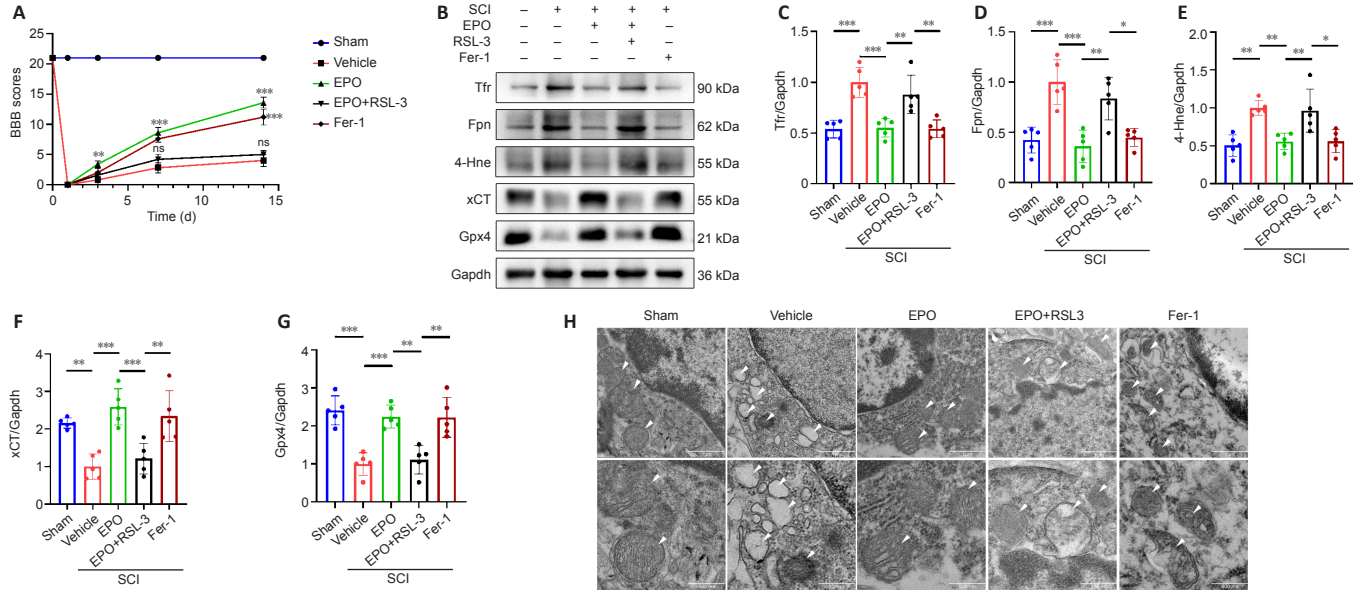

Figure 4 | **The effects of EPO in SCI are abolished by the ferroptosis activator RSL3.**
(A) BBB scores in the indicated groups. (B–G) Western blot and quantification of the indicated proteins from injured tissue at 14 dpi. Gapdh was used as the reference protein. All data are expressed as the mean ± SD ($n = 5$ in each group). $^*P < 0.05$, $^{**}P < 0.01$, $^{***}P < 0.001$ (one-way analysis of variance followed by Dunnett's multiple comparisons test). (H) Mitochondria from injured tissue were observed by transmission electron miscorscopy at 7 dpi. Shrunken mitochondria and cristae disappearance were identified as ferroptosis-like morphological changes. White arrows indicate the mitochondria. Scale bars: top, 1 μm; bottom, 500 nm. 4-Hne: 4-Hydroxynonenal; dpi: day(s) post injury; EPO: erythropoietin; Fer-1: ferrostatin-1; Fpn: ferroportin or solute carrier family 40 member 1; Gapdh: glyceraldehyde-3-phosphate dehydrogenase; Gpx4: glutathione peroxidase 4; ns: not significant; RSL3: (1S,3R)-RSL3; TEM: transmission electron microscope; SCI: spinal cord injury; Tfr: transferrin receptor; xCT: the solute carrier family 7 member 11.

EPO rescues RSL3-induced ferroptosis in PC12 cells

To more closely examine the effects of EPO on SCI-induced ferroptosis in rats, we performed *in vitro* experiments in PC12 cells. Cell viability assays of RSL3 treatment in PC12 cells were performed, and the IC50 of RSL3 at 24 hours was 10.21 μM (**Figure 6A**). We then examined the inhibitory effect of EPO at different concentrations (5, 10, 20, 40 IU/mL) against RSL3-induced ferroptosis. EPO at 40 IU/mL showed the most significant suppression on Tfr and 4-Hne (P = 0.006 and P = 0.003 respectively, relative to that at 0 IU/mL; **Figure 6B–D**). Therefore, RSL3 at 10 μM and EPO at 40 IU/mL were selected to establish the RSL3 + EPO group for the subsequent assays.

Loss of MMP is a feature of early ferroptosis (Chiu et al., 2009). MMP assay with JC-1 showed that the MMP of the RSL3 group decreased, and after treatment with EPO, the MMP was closer to that of the control group (**Figure 6E**). Moreover, FCM results showed that the number of JC-1 monomer-positive cells in the RSL3 + EPO group was significantly less than that of the RSL3 group (P < 0.001; **Figure 6F** and **G**). These results suggested that EPO may improve mitochondrial state in RSL3-treated PC12 cells.

As shown in **Figure 7A–D**, there was a significant reduction of 4-Hne and a significant increase of xCT and Gpx4 in the RSL3 + EPO group relative to the levels in the RSL3 group (4-Hne: P = 0.003; xCT: P = 0.048; Gpx4: P = 0.019). Immunofluorescence staining revealed stronger fluorescence intensity of xCT and Gpx4 and weaker 4-Hne in the RSL3 + EPO group relative to the RSL3 group (**Figure 7E–J**). These results suggested that EPO protected PC12 cells from RSL3-induced ferroptosis via upregulating xCT and Gpx4.

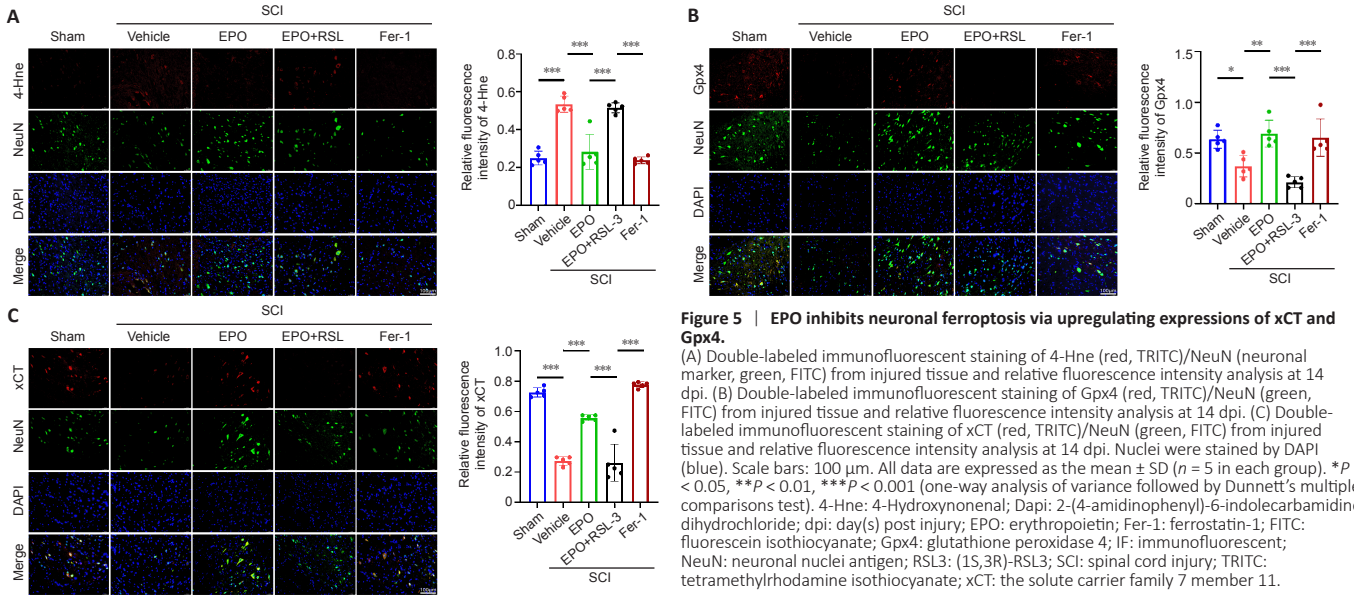

Figure 5 | EPO inhibits neuronal ferroptosis via upregulating expressions of xCT and Gpx4.

(A) Double-labeled immunofluorescent staining of 4-Hne (red, TRITC)/NeuN (neuronal marker, green, FITC) from injured tissue and relative fluorescence intensity analysis at 14 dpi. (B) Double-labeled immunofluorescent staining of Gpx4 (red, TRITC)/NeuN (green, FITC) from injured tissue and relative fluorescence intensity analysis at 14 dpi. (C) Double-labeled immunofluorescent staining of xCT (red, TRITC)/NeuN (green, FITC) from injured tissue and relative fluorescence intensity analysis at 14 dpi. Nuclei were stained by DAPI (blue). Scale bars: 100 μm. All data are expressed as the mean ± SD (n = 5 in each group). *P < 0.05, **P < 0.01, ***P < 0.001 (one-way analysis of variance followed by Dunnett's multiple comparisons test). 4-Hne: 4-Hydroxynonenal; Dapi: 2-(4-amidinophenyl)-6-indolecarbamidine dihydrochloride; dpi: day(s) post injury; EPO: erythropoietin; Fer-1: ferrostatin-1; FITC: fluorescein isothiocyanate; Gpx4: glutathione peroxidase 4; IF: immunofluorescent; NeuN: neuronal nuclei antigen; RSL3: (1S,3R)-RSL3; SCI: spinal cord injury; TRITC: tetramethylrhodamine isothiocyanate; xCT: the solute carrier family 7 member 11.

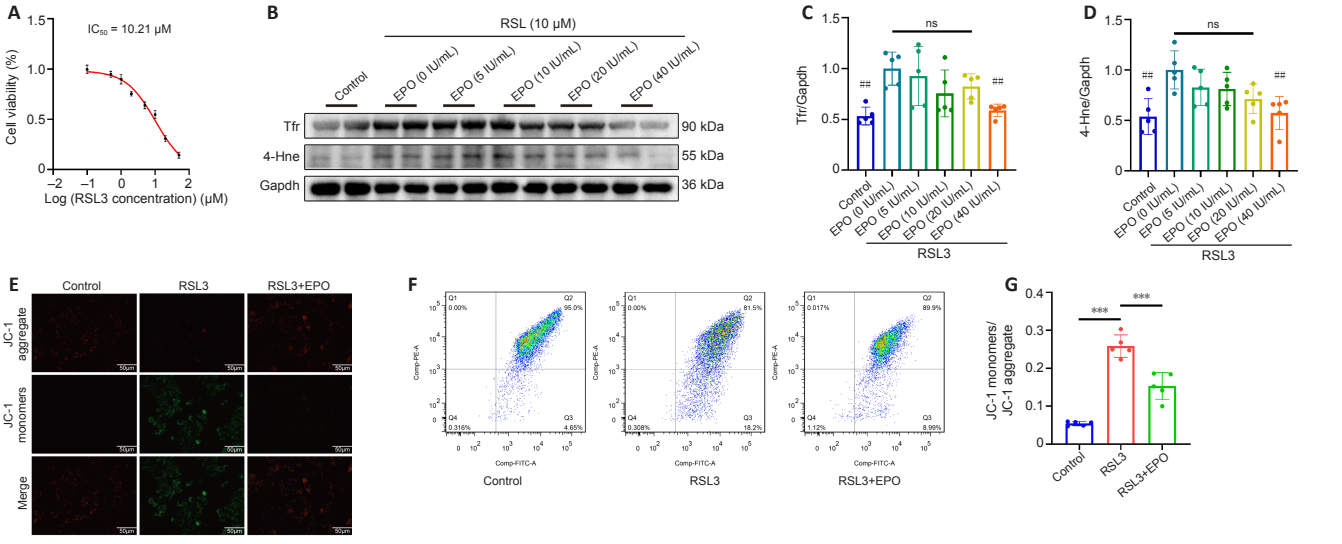

Figure 6 | EPO alleviates RSL3-induced ferroptosis in PC12 cells.

(A) Cell viability test of PC12 cells treated with RSL3 for 24 hours. The IC_{50} of RSL3 was 10.21 μM. (B–D) Western blot and quantitative analysis of PC12 cells treated as indicated. (E) Representative fluorescence images of JC-1 aggregate$^+$ (red)/JC-1 monomer$^+$ (green) PC12 cells. JC-1 aggregate (red) indicates normal MMP; JC-1 monomer (green) indicates depolarized MMP. Scale bars: 50 μm. (F, G) Flow cytometry and quantitative analysis of MMP in PC12 cells. Quadrant 2 (Q2) represents JC-1 aggregate-positive cells and quadrant 3 (Q3) represents JC-1 monomer-positive cells. All data are expressed as the mean ± SD (n = 5 in each group). ***P < 0.001 (in G), ##P < 0.01 (*vs.* EPO group in C and D) (one-way analysis of variance followed by Dunnett's multiple comparisons test). 4-Hne: 4-Hydroxynonenal; EPO: erythropoietin; FCM: flow cytometry; Gapdh: glyceraldehyde-3-phosphate dehydrogenase; IC50: half maximal inhibitory concentration; MMP: mitochondrial membrane potential; RSL3: (1S,3R)-RSL3; Tfr: transferrin receptor.

Discussion

In the present study, we used a rat SCI model and PC12 cell model to investigate the mechanism of the neuroprotective effects of EPO and potential involvement of ferroptosis. We used two different doses of EPO to treat SCI rats, and both doses of EPO improved the hindlimb function recovery and spinal cord regeneration. Several characteristics of ferroptosis, including iron overload, ROS accumulation, lipid peroxidation, GSH depletion and ferroptosis biomarkers (Dixon et al., 2012; Zheng et al., 2020), were rescued by EPO. High dose of EPO exhibited a stronger inhibitory effect on SCI-induced ferroptosis relative to low EPO dose. RSL3 is a Gpx4-targeting ferroptosis inducer (Shin et al., 2018), and Fer-1 is a potent and selective ferroptosis inhibitor (Liu et al., 2020a). The efficacy of EPO was similar to that of Fer-1, and the effects of EPO disappeared when co-treated with RSL3. The RSL3-induced lipid peroxidation and exhaustion of xCT and Gpx4 in PC12 cells was reversed by EPO.

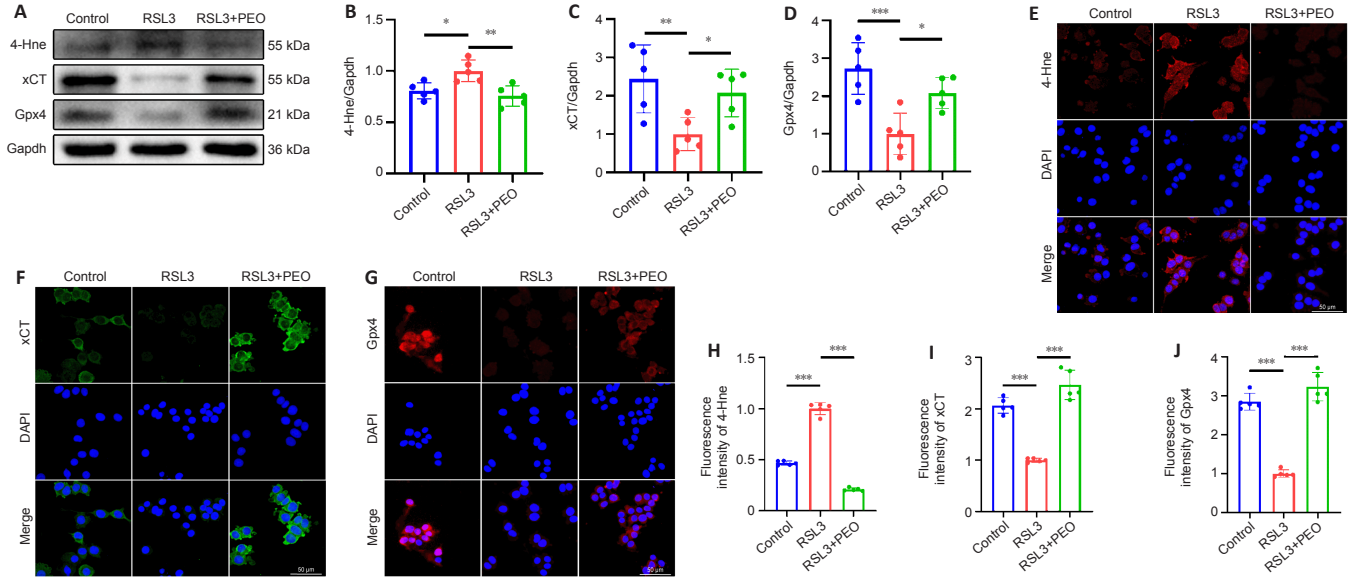

Figure 7 | **EPO increases expressions of xCT and Gpx4 against RSL3-induced ferroptosis in PC12 cells.**
(A–D) Western blot and quantification of the indicated proteins in PC12 cells. Gapdh was used as the reference protein. (E) Representative immunofluorescence images of 4-Hne (red, TRITC) in PC12 cells. (F) Representative immunofluorescence images of xCT (green, FITC) in PC12 cells. (F) Representative immunofluorescence images of Gpx4 (red, TRITC) in PC12 cells. Nuclei were stained by DAPI (blue). Scale bars: 50 μm. (H–J) Quantitative analysis of fluorescence intensity. All data are expressed as the mean ± SD (n = 5 in each group). *P < 0.05, **P < 0.01, ***P < 0.001 (one-way analysis of variance followed by Dunnett's multiple comparisons test). 4-Hne: 4-Hydroxynonenal; Dapi: 2-(4-amidinophenyl)-6-indolecarbamidine dihydrochloride; EPO: erythropoietin; FITC: fluorescein isothiocyanate; Gapdh: glyceraldehyde-3-phosphate dehydrogenase; Gpx4: glutathione peroxidase 4; IF: immunofluorescent; RSL3: (1S,3R)-RSL3; TRITC: tetramethylrhodamine isothiocyanate; xCT: the solute carrier family 7 member 11.

BBB scale and footprint analysis are two classical methods to evaluate the neurological function recovery of SCI rats (Basso et al., 1995; Wen et al., 2015). Our results demonstrated that EPO promoted the BBB scores and stride distance after SCI even with a low dose. The improvement in hindlimb motor function was consistent with the findings of histology and MRI scan. Tissue necrosis and neuron loss were relieved by both doses of EPO. The MRI scan was performed at 14 dpi; therefore, we speculate that the high signal on sagittal T2-weighted within spinal cord did not represent the edema but the ischemia/reperfusion injury, which is an important pathogenic factor contributing to neurological deterioration (Liao et al., 2020). This area of high signal was significantly reduced by EPO treatment.

Iron overload is a characteristic and driving factor of SCI-induced ferroptosis (Dixon et al., 2012; Jing et al., 2021). Erythrocyte lysis following SCI causes the sharp increase of ferric ion (Fe^{3+}) locally. Fe^{3+} is transported into cells mediated by Tfr and degraded to the highly reactive Fe^{2+} under the action of the six-transmembrane protein of prostate 3, which induces ferroptosis through the Fenton reaction (Chen et al., 2020). When intracellular iron accumulates, Fth and Fpn, which function in iron storage and export, respectively, are upregulated (Rui et al., 2021). Therefore, Tfr, Fpn and Fth are regarded as the indicators of ferroptosis. We found that Tfr, Fpn and Fth were significantly decreased in response to EPO high dose and iron overload was alleviated with EPO. Therefore, high dose of EPO might stabilize the cellular iron metabolism in SCI-induced ferroptosis.

Ferroptosis is also characterized by ROS accumulation and lipid peroxidation (Zheng et al., 2020). Fenton reaction catalyzed by iron generates a large amount of ROS, which leads to cell death (Hassannia et al., 2019). Increased polyunsaturated fatty acid is a cause of lipid peroxidation (Hong et al., 2017), and Acsl4 is one of the key enzymes involved in polyunsaturated fatty acid formation (Doll et al., 2017). Dehydrogenation of polyunsaturated fatty acids forms phospholipid hydroperoxide, which is decomposed to 4-Hne and MDA (Hassannia et al., 2019). As the end products of lipid peroxidation, 4-Hne and MDA reflect the degree of ferroptosis. In our study, we found weaker fluorescence of ROS, downregulated expression of 4-Hne and lower level of MDA in response to EPO. These findings suggested a reduction of ferroptosis in EPO groups.

Gpx4 plays an essential role in ferroptotic regulation (Xie et al., 2016). Polyunsaturated fatty acid forms phospholipid hydroperoxide that is converted by Gpx4 to phosphatidylcholine (PL-alcohol), which does not exert lipid radical activity. Therefore, Gpx4 can prevent lipid peroxidation and suppress ferroptosis (Proneth and Conrad, 2019). GSH is a cofactor for Gpx4 and important for maintaining Gpx4 activity (Chen et al., 2020). Cysteine is an indispensable substrate for GSH synthesis. Cellular cysteine is transported into cells via xCT, which comprises two subunits: solute carrier family 3 member 2 and the solute carrier family 7 member 11 (Bordini et al., 2020). We observed reduction of GSH, xCT and Gpx4 in the vehicle group after SCI, which was consistent with previous reports (Zhang et al., 2019, 2020). However, we found the markedly augmentated GSH and upregulated mRNA and protein of xCT and Gpx4 in the two EPO groups.

While both doses of EPO exhibited neuroprotective and anti-ferroptotic effects, there were no significant differences between the groups in ferroptosis biomarker expression. Tfr, Acsl4, Fpn and Fth expressions decreased significantly with high EPO dose not with low dose. Results from the behavior test, ROS, iron content and MDA assays in the high dose group were superior to those in the low dose group. Therefore, low EPO dose exhibited a strong effect on activating xCT and Gpx4 , but it was not enough for maintaining iron homeostasis and promoting functional recovery. Considering the stronger effects in the high dose group, we used the high EPO dose for the second animal experiments.

The neuroprotective and anti-ferroptotic effects of EPO were largely offset by RSL3 *in vivo*. The decreased BBB scores in EPO + RSL3 group could partly explain the results of double-labeled fluorescence staining: EPO promoted the neuronal xCT and Gpx4 to alleviate ferroptosis while RSL3 reproduced neuronal ferroptosis. The biomarkers related to ferroptosis (Tfr, Fpn and 4-Hne) were reupregulated and the enhanced effects of EPO on xCT and Gpx4 were abolished in the EPO + RSL3 group. Additionally, the ferroptosis inhibitor Fer-1 and EPO exerted the similar effects on SCI rats. *In vitro*, we validated the promotion of EPO on xCT and Gpx4 using EPO to rescue RSL3-induced ferroptosis in PC12 cells.

Mitochondrial dysfunction is inextricably linked to ferroptosis. Shrunken mitochondrial and disappeared cristae are morphological characteristics of SCI-induced ferroptosis (Zhang et al., 2019; Ge et al., 2021). MMP is an effective biomarker to assess the function of the mitochondria (Galley et al., 2017) and decreased MMP is one of the early symbols involved in ferroptosis (Chiu et al., 2009; Wu et al., 2018; Ge et al., 2021). We found that EPO and Fer-1 alleviated the mitochondria damage after SCI as shown in TEM results. Fluorescence and flow cytometry indicated that EPO contributes to the recovery of decreased MMP in ferroptosis.

This study has several limitations. First, the sample size was relatively small, and an increased sample size should be considered to improve the accuracy of our study. Second, primary neuronal cells should be used to better understand the neuroprotective effect of EPO.

In conclusion, we examined the effects of EPO on preventing SCI-induced ferroptosis in a rat SCI model and determined the facilitatory effects of EPO on xCT and Gpx4 *in vivo* and *in vitro*. These findings provide new insights into the neuroprotective effect of EPO in SCI, and the anti-ferroptotic effect of EPO makes it a potential therapeutic strategy for clinical improvement of SCI.

Acknowledgments: *We thank Prof. Xuan-Ming Shi from the School of Basic Medical Sciences of Anhui Medical University for his valuable advice on graphing and writing. We also thank Dr. Yin-Feng Qian and Dr. Fu-Jun Liu from the Laboratory of Functional Imaging and Molecular Imaging (The First Affiliated Hospital of Anhui Medical University) for providing technical support on magnetic resonance imaging.*
Author contributions: *Study design and concept: YK and ZSY; animal experiment implementation: YK, RZ and SL; rat management: YK; cell experiment implementation: YK, RZ, SL and WSS; literature retrieval: KPQ and HT; data analysis and manuscript preparation: YK, RZ and ZSY; manuscript*

review: YK and ZSY. All authors approved the final version of the manuscript.

Conflicts of interest: *We declare that the research was conducted in the absence of any commercial or financial relationships that could be construed as a potential conflict of interest.*

Availability of data and materials: *All data generated or analyzed during this study are included in this published article and its supplementary information files.*

Open peer reviewers: *Ming Li, Peking University People's Hospital, China; Michel Edwar-Mickael, Institute of Animal Biotechnology and Genetics, Polish Academy of Science, Poland.*

Additional file: *Open peer review reports 1 and 2.*

References

Basso DM, Beattie MS, Bresnahan JC (1995) A sensitive and reliable locomotor rating scale for open field testing in rats. J Neurotrauma 12:1-21.

Bordini J, Morisi F, Cerruti F, Cascio P, Camaschella C, Ghia P, Campanella A (2020) Iron causes lipid oxidation and inhibits proteasome function in multiple myeloma cells: a proof of concept for novel combination therapies. Cancers (Basel) 12:970.

Cao J, Chen X, Jiang L, Lu B, Yuan M, Zhu D, Zhu H, He Q, Yang B, Ying M (2020) DJ-1 suppresses ferroptosis through preserving the activity of S-adenosyl homocysteine hydrolase. Nat Commun 11:1251.

Chen Y, Liu S, Li J, Li Z, Quan J, Liu X, Tang Y, Liu B (2020) The latest view on the mechanism of ferroptosis and its research progress in spinal cord injury. Oxid Med Cell Longev 2020:6375938.

Cheng J, Xu T, Xun C, Guo H, Cao R, Gao S, Sheng W (2021) Carnosic acid protects against ferroptosis in PC12 cells exposed to erastin through activation of Nrf2 pathway. Life Sci 266:118905.

Chiu HY, Tsao LY, Yang RC (2009) Heat-shock response protects peripheral blood mononuclear cells (PBMCs) from hydrogen peroxide-induced mitochondrial disturbance. Cell Stress Chaperones 14:207-217.

Cui Y, Zhang Y, Zhao X, Shao L, Liu G, Sun C, Xu R, Zhang Z (2021) ACSL4 exacerbates ischemic stroke by promoting ferroptosis-induced brain injury and neuroinflammation. Brain Behav Immun 93:312-321.

Dietz V, Fouad K (2014) Restoration of sensorimotor functions after spinal cord injury. Brain 137:654-667.

Dixon SJ, Lemberg KM, Lamprecht MR, Skouta R, Zaitsev EM, Gleason CE, Patel DN, Bauer AJ, Cantley AM, Yang WS, Morrison B, 3rd, Stockwell BR (2012) Ferroptosis: an iron-dependent form of nonapoptotic cell death. Cell 149:1060-1072.

Doll S, Proneth B, Tyurina YY, Panzilius E, Kobayashi S, Ingold I, Irmler M, Beckers J, Aichler M, Walch A, Prokisch H, Trümbach D, Mao G, Qu F, Bayir H, Füllekrug J, Scheel CH, Wurst W, Schick JA, Kagan VE, et al. (2017) ACSL4 dictates ferroptosis sensitivity by shaping cellular lipid composition. Nat Chem Biol 13:91-98.

Feng H, Schorpp K, Jin J, Yozwiak CE, Hoffstrom BG, Decker AM, Rajbhandari P, Stokes ME, Bender HG, Csuka JM, Upadhyayula PS, Canoll P, Uchida K, Soni RK, Hadian K, Stockwell BR (2020) Transferrin receptor is a specific ferroptosis marker. Cell Rep 30:3411-3423.e7.

Feng Z, Min L, Chen H, Deng W, Tan M, Liu H, Hou J (2021) Iron overload in the motor cortex induces neuronal ferroptosis following spinal cord injury. Redox Biol 43:101984.

Ferrero SL, Brady TD, Dugan VP, Armstrong JE, Hubscher CH, Johnson RD (2015) Effects of lateral funiculus sparing, spinal lesion level, and gender on recovery of bladder voiding reflexes and hematuria in rats. J Neurotrauma 32:200-208.

Freitag MT, Márton G, Pajer K, Hartmann J, Walder N, Rossmann M, Parzer P, Redl H, Nógrádi A, Stieltjes B (2015) Monitoring of short-term erythropoietin therapy in rats with acute spinal cord injury using manganese-enhanced magnetic resonance imaging. J Neuroimaging 25:582-589.

Galley HF, McCormick B, Wilson KL, Lowes DA, Colvin L, Torsney C (2017) Melatonin limits paclitaxel-induced mitochondrial dysfunction in vitro and protects against paclitaxel-induced neuropathic pain in the rat. J Pineal Res 63:e12444.

Ge H, Xue X, Xian J, Yuan L, Wang L, Zou Y, Zhong J, Jiang Z, Shi J, Chen T, Su H, Feng H, Hu S (2022) Ferrostatin-1 alleviates white matter injury via decreasing ferroptosis following spinal cord injury. Mol Neurobiol 59:161-176.

Ge MH, Tian H, Mao L, Li DY, Lin JQ, Hu HS, Huang SC, Zhang CJ, Mei XF (2021) Zinc attenuates ferroptosis and promotes functional recovery in contusion spinal cord injury by activating Nrf2/GPX4 defense pathway. CNS Neurosci Ther 27:1023-1040.

Gong QY, Cai L, Jing Y, Wang W, Yang DX, Chen SW, Tian HL (2022) Urolithin A alleviates blood-brain barrier disruption and attenuates neuronal apoptosis following traumatic brain injury in mice. Neural Regen Res 17:2007-2013.

Grasso G, Sfacteria A, Passalacqua M, Morabito A, Buemi M, Macrì B, Brines ML, Tomasello F (2005) Erythropoietin and erythropoietin receptor expression after experimental spinal cord injury encourages therapy by exogenous erythropoietin. Neurosurgery 56:821-827; discussion 821-827.

Greene LA, Tischler AS (1976) Establishment of a noradrenergic clonal line of rat adrenal pheochromocytoma cells which respond to nerve growth factor. Proc Natl Acad Sci U S A 73:2424-2428.

Hassannia B, Vandenabeele P, Vanden Berghe T (2019) Targeting ferroptosis to iron out cancer. Cancer Cell 35:830-849.

He Z, Zhou Y, Huang Y, Wang Q, Zheng B, Zhang H, Li J, Liu Y, Wu F, Zhang X, Tong S, Wang M, Wang Z, He H, Xu H, Xiao J (2017) Dl-3-n-butylphthalide improves functional recovery in rats with spinal cord injury by inhibiting endoplasmic reticulum stress-induced apoptosis. Am J Transl Res 9:1075-1087.

Hong M, Li S, Wang N, Tan HY, Cheung F, Feng Y (2017) A biomedical investigation of the hepatoprotective effect of radix salviae miltiorrhizae and network pharmacology-based prediction of the active compounds and molecular targets. Int J Mol Sci 18:620.

Jing X, Du T, Li T, Yang X, Wang G, Liu X, Jiang Z, Cui X (2021) The detrimental effect of iron on OA chondrocytes: Importance of pro-inflammatory cytokines induced iron influx and oxidative stress. J Cell Mol Med 25:5671-5680.

Jhelum P, David S (2022) Ferroptosis: copper-iron connection in cuprizone-induced demyelination. Neural Regen Res 17:89-90.

Kremer DM, Nelson BS, Lin L, Yarosz EL, Halbrook CJ, Kerk SA, Sajjakulnukit P, Myers A, Thurston G, Hou SW, Carpenter ES, Andren AC, Nwosu ZC, Cusmano N, Wisner S, Mbah NE, Shan M, Das NK, Magnuson B, Little AC, et al. (2021) GOT1 inhibition promotes pancreatic cancer cell death by ferroptosis. Nat Commun 12:4860.

Larpthaveesarp A, Georgevits M, Ferriero DM, Gonzalez FF (2016) Delayed erythropoietin therapy improves histological and behavioral outcomes after transient neonatal stroke. Neurobiol Dis 93:57-63.

Li J, Guo W, Xiong M, Han H, Chen J, Mao D, Tang B, Yu H, Zeng Y (2015) Effect of SDF-1/CXCR4 axis on the migration of transplanted bone mesenchymal stem cells mobilized by erythropoietin toward lesion sites following spinal cord injury. Int J Mol Med 36:1205-1214.

Liao YX, He SS, He ZM (2020) 'White cord syndrome', a rare but disastrous complication of transient paralysis after posterior cervical decompression for severe cervical spondylotic myelopathy and spinal stenosis: A case report. Exp Ther Med 20:90.

Lin CW, Chen B, Huang KL, Dai YS, Teng HL (2016) Inhibition of Autophagy by Estradiol Promotes Locomotor Recovery after Spinal Cord Injury in Rats. Neurosci Bull 32:137-144.

Lipinski MM, Wu J, Faden AI, Sarkar C (2015) Function and mechanisms of autophagy in brain and spinal cord trauma. Antioxid Redox Signal 23:565-577.

Liu P, Feng Y, Li H, Chen X, Wang G, Xu S, Li Y, Zhao L (2020a) Ferrostatin-1 alleviates lipopolysaccharide-induced acute lung injury via inhibiting ferroptosis. Cell Mol Biol Lett 25:10.

Liu Y, Zeng L, Yang Y, Chen C, Wang D, Wang H (2020b) Acyl-CoA thioesterase 1 prevents cardiomyocytes from Doxorubicin-induced ferroptosis via shaping the lipid composition. Cell Death Dis 11:756.

Livak KJ, Schmittgen TD (2001) Analysis of relative gene expression data using real-time quantitative PCR and the 2(-Delta Delta C(T)) Method. Methods 25:402-408.

Lu Y, Yang Q, Su Y, Ji Y, Li G, Yang X, Xu L, Lu Z, Dong J, Wu Y, Bei JX, Pan C, Gu X, Li B (2021) MYCN mediates TFRC-dependent ferroptosis and reveals vulnerabilities in neuroblastoma. Cell Death Dis 12:511.

Nagai A, Nakagawa E, Choi HB, Hatori K, Kobayashi S, Kim SU (2001) Erythropoietin and erythropoietin receptors in human CNS neurons, astrocytes, microglia, and oligodendrocytes grown in culture. J Neuropathol Exp Neurol 60:386-392.

Proneth B, Conrad M (2019) Ferroptosis and necroinflammation, a yet poorly explored link. Cell Death Differ 26:14-24.

Roseti C, Cifelli P, Ruffolo G, Barbieri E, Guescini M, Esposito V, Di Gennaro G, Limatola C, Giovannelli A, Aronica E, Palma E (2020) Erythropoietin increases GABA(A) currents in human cortex from TLE patients. Neuroscience 439:153-162.

Rui T, Wang H, Li Q, Cheng Y, Gao Y, Fang X, Ma X, Chen G, Gao C, Gu Z, Song S, Zhang J, Wang C, Wang Z, Wang T, Zhang M, Min J, Chen X, Tao L, Wang F, et al. (2021) Deletion of ferritin H in neurons counteracts the protective effect of melatonin against traumatic brain injury-induced ferroptosis. J Pineal Res 70:e12704.

Schneider CA, Rasband WS, Eliceiri KW (2012) NIH Image to ImageJ: 25 years of image analysis. Nat Methods 9:671-675.

Shen LM, Song ZW, Hua Y, Chao X, Liu JB (2017) miR-181d-5p promotes neurite outgrowth in PC12 Cells via PI3K/Akt pathway. CNS Neurosci Ther 23:894-906.

Shi Z, Yuan S, Shi L, Li J, Ning G, Kong X, Feng S (2021) Programmed cell death in spinal cord injury pathogenesis and therapy. Cell Prolif 54:e12992.

Shin D, Kim EH, Lee J, Roh JL (2018) Nrf2 inhibition reverses resistance to GPX4 inhibitor-induced ferroptosis in head and neck cancer. Free Radic Biol Med 129:454-462.

Sun J, Martin JM, Vanderpoel V, Sumbria RK (2019) The promises and challenges of erythropoietin for treatment of Alzheimer's disease. Neuromolecular Med 21:12-24.

Ureña-Guerrero ME, Castañeda-Cabral JL, Rivera-Cervantes MC, Macias-Velez RJ, Jarero-Basulto JJ, Gudiño-Cabrera G, Beas-Zárate C (2020) Neuroprotective and neurorestorative effects of Epo and VEGF: perspectives for new therapeutic approaches to neurological diseases. Curr Pharm Des 26:1263-1276.

Wang Y, Wang H, Tao Y, Zhang S, Wang J, Feng X (2014) Necroptosis inhibitor necrostatin-1 promotes cell protection and physiological function in traumatic spinal cord injury. Neuroscience 266:91-101.

Wen J, Sun D, Tan J, Young W (2015) A consistent, quantifiable, and graded rat lumbosacral spinal cord injury model. J Neurotrauma 32:875-892.

Wu C, Zhao W, Yu J, Li S, Lin L, Chen X (2018) Induction of ferroptosis and mitochondrial dysfunction by oxidative stress in PC12 cells. Sci Rep 8:574.

Wu H, Liu X, Jaenisch R, Lodish HF (1995) Generation of committed erythroid BFU-E and CFU-E progenitors does not require erythropoietin or the erythropoietin receptor. Cell 83:59-67.

Xie Y, Hou W, Song X, Yu Y, Huang J, Sun X, Kang R, Tang D (2016) Ferroptosis: process and function. Cell Death Differ 23:369-379.

Xu S, Wang J, Zhong J, Shao M, Jiang J, Song J, Zhu W, Zhang F, Xu H, Xu G, Zhang Y, Ma X, Lyu F (2021) CD73 alleviates GSDMD-mediated microglia pyroptosis in spinal cord injury through PI3K/AKT/Foxo1 signaling. Clin Transl Med 11:e269.

Yamanaka K, Eldeiry M, Aftab M, Ryan TJ, Mares J, Meng X, Weyant MJ, Cleveland JC, Jr., Fullerton DA, Reece TB (2018) Synergistic reduction of apoptosis with diazoxide and erythropoietin in spinal cord ischemic injury. Ann Thorac Surg 106:1751-1758.

Yang J, Mo J, Dai J, Ye C, Cen W, Zheng X, Jiang L, Ye L (2021) Cetuximab promotes RSL3-induced ferroptosis by suppressing the Nrf2/HO-1 signalling pathway in KRAS mutant colorectal cancer. Cell Death Dis 12:1079.

Yong C, Arnold PM, Zoubine MN, Citron BA, Watanabe I, Berman NE, Festoff BW (1998) Apoptosis in cellular compartments of rat spinal cord after severe contusion injury. J Neurotrauma 15:459-472.

Zhang Y, Fan BY, Pang YL, Shen WY, Wang X, Zhao CX, Li WX, Liu C, Kong XH, Ning GZ, Feng SQ, Yao X (2020) Neuroprotective effect of deferoxamine on erastininduced ferroptosis in primary cortical neurons. Neural Regen Res 15:1539-1545.

Zhang Y, Sun C, Zhao C, Hao J, Zhang Y, Fan B, Li B, Duan H, Liu C, Kong X, Wu P, Yao X, Feng S (2019) Ferroptosis inhibitor SRS 16-86 attenuates ferroptosis and promotes functional recovery in contusion spinal cord injury. Brain Res 1706:48-57.

Zheng Z, Tang D, Zhao L, Li W, Han J, Hu B, Nie G, He Y (2020) Liproxstatin-1 protects hair cell-like HEI-OC1 cells and cochlear hair cells against neomycin ototoxicity. Oxid Med Cell Longev 2020:1782659.

Zhong L, Zhang H, Ding ZF, Li J, Lv JW, Pan ZJ, Xu DX, Yin ZS (2020) Erythropoietin-induced autophagy protects against spinal cord injury and improves neurological function via the extracellular-regulated protein kinase signaling pathway. Mol Neurobiol 57:3993-4006.

Zhou X, Zheng Y, Sun W, Zhang Z, Liu J, Yang W, Yuan W, Yi Y, Wang J, Liu J (2021) D-mannose alleviates osteoarthritis progression by inhibiting chondrocyte ferroptosis in a HIF-2α-dependent manner. Cell Prolif 54:e13134.

P-Reviewers: Li M, Edwar-Mickael E; C-Editor: Zhao M; S-Editors: Yu J, Li CH; L-Editors: Wolf GW, Song LP; T-Editor: Jia Y